Karlsruhe Institute of Technology

Deterministic models for pressure-tilt-coupling

Geophysical Institute (GPI), Black Forest Observatory (BFO)

Thomas Forbriger and Walter Zürn | 4.11.2022

Preview

1. The trigger for this presentation: KAGRA's seismic response to atmospheric pressure signal from Hunga Tonga eruption
2. Black Forest Observatory (BFO)
3. Levels of common tilt noise floor
4. Coupling mechanisms: LDT and TWT
5. Evidence from horizontal component data analysis
6. Application to Hunga Tonga Lamb- and sound-wave
7. The traveling wave model above 10 mHz
8. Conclusions

The trigger for this presentation

KAGRA seismic response to Hunga Tonga eruption

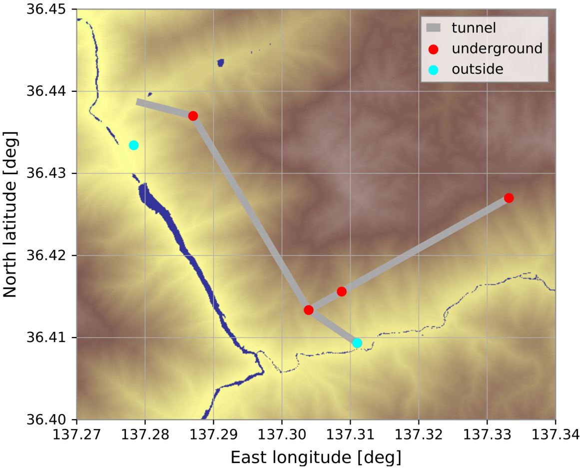

Washimi *et al.* (2022, arXiv:2206.14396v3)

The trigger for this presentation

KAGRA seismic response to Hunga Tonga eruption

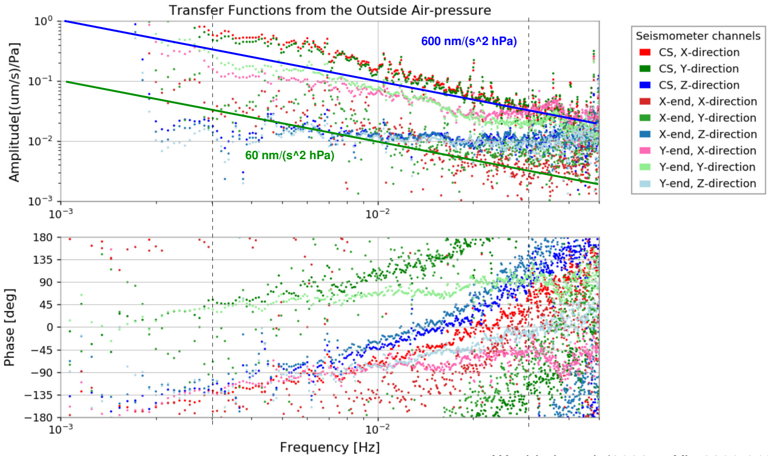

Washimi *et al.* (2022, arXiv:2206.14396v3)

The trigger for this presentation

- The nature of the frequency dependence (rather continuous) points to a deterministic coupling to external pressure.
- Response of KAGRA seismometers is significantly larger than expected (by at least a factor of 10).
- Due to large inter-sensor distances the phase response cannot easily be attributed to a dominating mechanism.

Questions raised

- Is the atmospherically induced tilt-background an issue for ET?
- At which level is the tilt-background to be expected?
- What are the dominating mechanisms controlling the level of the tilt background?
- Does the effect of loading at the Earth's surface dominate?
- How strong is the effect of pressure fluctuations in the cavern?

Black Forest Observatory (BFO)

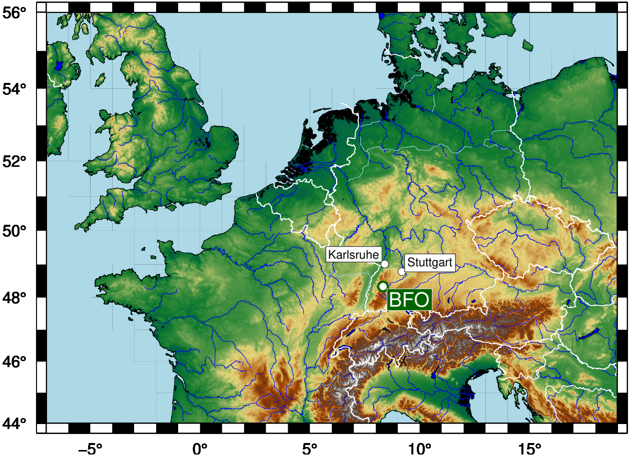

Black Forest Observatory (BFO)

Cross-section of local geology

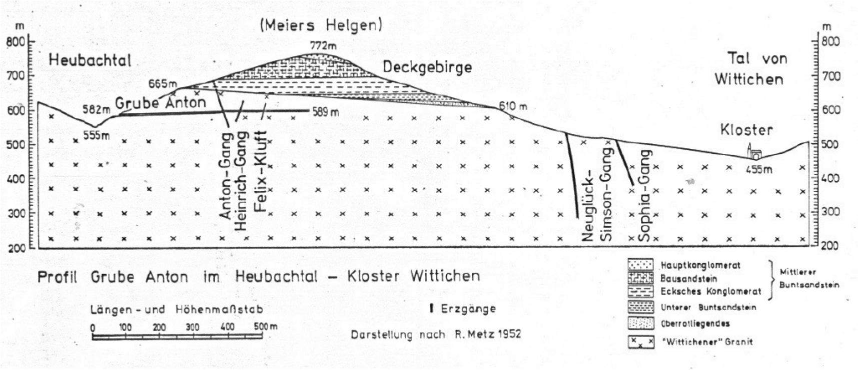

Common noise floor

Low noise models

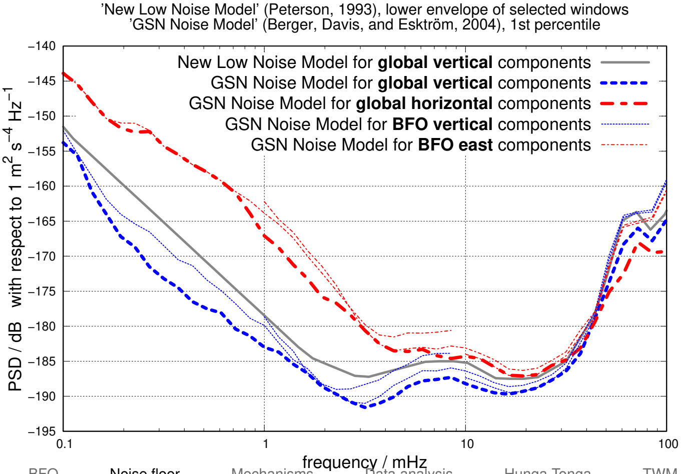

Common noise floor

Horizontal component background signals

Karlsruhe Institute of Technology

Signal background as observed at BFO caused by permanent natural processes (not including earthquakes or volcanic eruptions)

- tidal deformation (12 h, 24 h)
  50 nrad equivalent to 500 $\mathrm{nm\,s^{-2}}$
- atmospherically induced tilt (0.3 mHz to 10 mHz)
  5 nrad equivalent to 50 $\mathrm{nm\,s^{-2}}$
- atmospherically induced acceleration (3 mHz to 40 mHz)
  20 $\mathrm{nm\,s^{-2}}$
- marine microseisms (50 mHz to 200 mHz)
  30 $\mathrm{nm\,s^{-2}}$ to 1 $\mathrm{\mu m\,s^{-2}}$
  inertial acceleration dominates
  tilt does not exceed 1 nrad

Noise caused by the atmosphere

period band 100 s to 3600 s

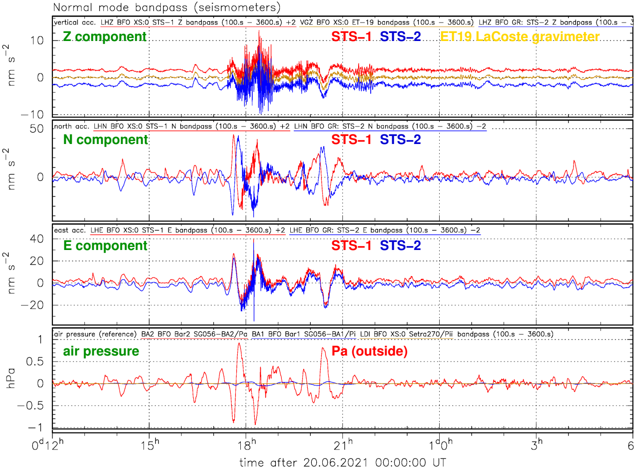

20.06.2021 17:05:51 M6.4 South of Kermadec Islands

Coupling mechanisms: LDT and TWT

Tilt-coupled gravity

Karlsruhe Institute of Technology

Response to tilt

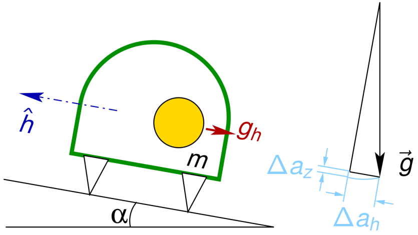

horizontal component

first order effect; $\Delta a_\mathrm{h} \approx |\vec{g}|\,\alpha$

vertical component

second order effect; $\Delta a_z \approx |\vec{g}|\,\alpha^2/2$

$\alpha \approx 0.000\,000\,001\,\mathrm{rad}$

$|\vec{g}| \approx 10\,000\,000\,000\,\mathrm{nm\,s^{-2}}$

Coupling mechanisms: LDT and TWT

'Local deformation tilt' (LDT): cavity deformation

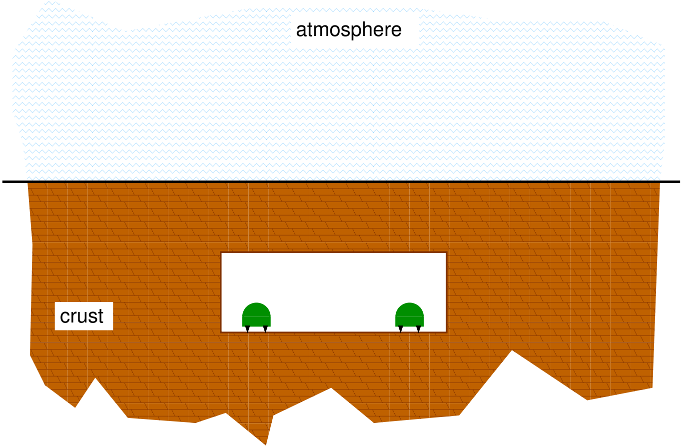

LDT as defined by Zürn *et al.* (2007, GJI, vol. 171, 780–796)

Coupling mechanisms: LDT and TWT

’Local deformation tilt’ (LDT): cavity deformation

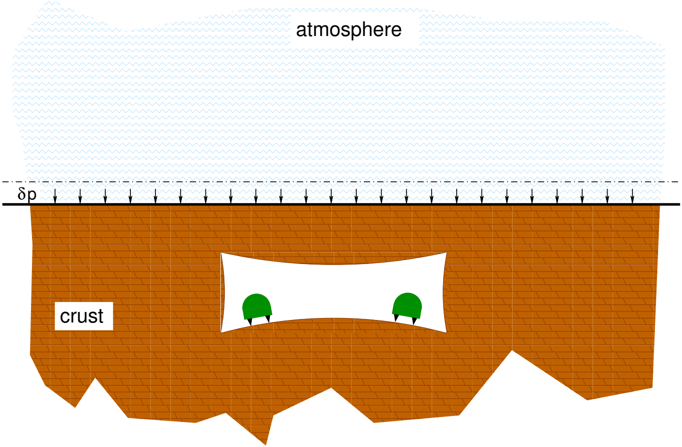

LDT as defined by Zürn *et al.* (2007, GJI, vol. 171, 780–796)

Coupling mechanisms: LDT and TWT

’Traveling wave tilt’ (TWT): horizontal gradient

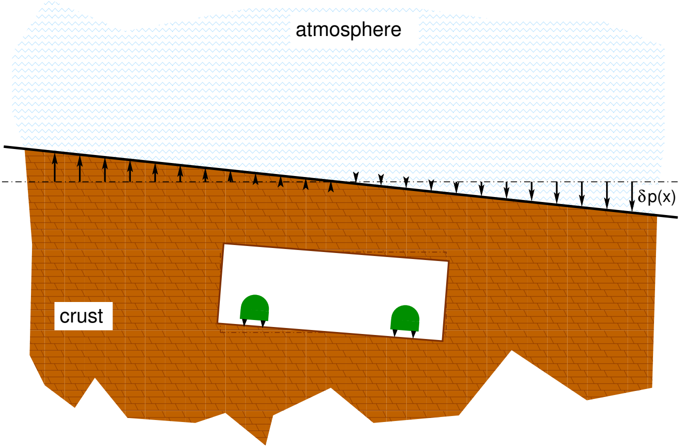

TWT as defined by Zürn *et al.* (2007, GJI, vol. 171, 780–796)

Evidence from recorded data

Instruments selected for this study

Karlsruhe Institute of Technology

Black Forest Observatory (BFO)

Most sensors are installed subsurface
in the gallery of a former silver mine.

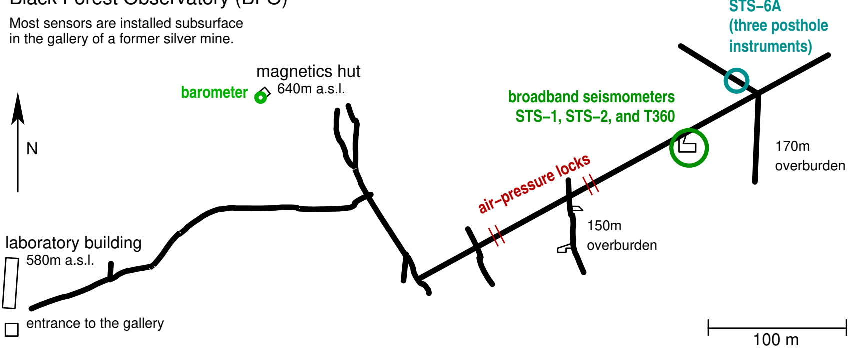

Evidence from recorded data

Instruments selected for this study
Seismometer vault at BFO

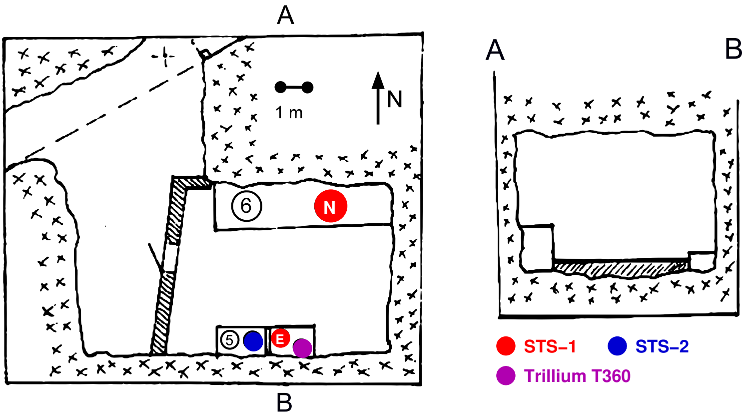

Evidence from recorded data

Joint regression

$$a_h(t) = c_p\, p(t) + c_{HT}\, \mathrm{HT}\,[p(t)] + r(t)$$

Minimize $r(t)$ in a least squares sense by adjusting c_p and c_{HT}.

$a_h(t)$: horizontal acceleration
$p(t)$: air pressure
c_p: accounts for LDT

$r(t)$: residual
$\mathrm{HT}\,[p(t)]$: Hilbert transform of $p(t)$
c_{HT}: accounts for TWT

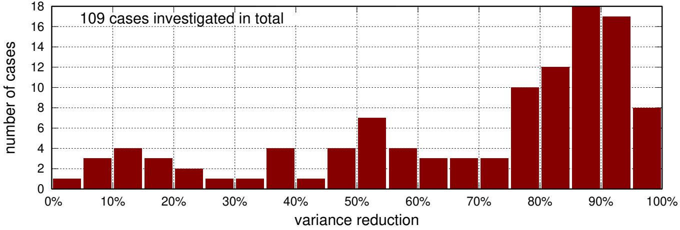

Zürn *et al.* (2021, GJI, vol. 228, 927–943)

Evidence from recorded data

Example of joint regression

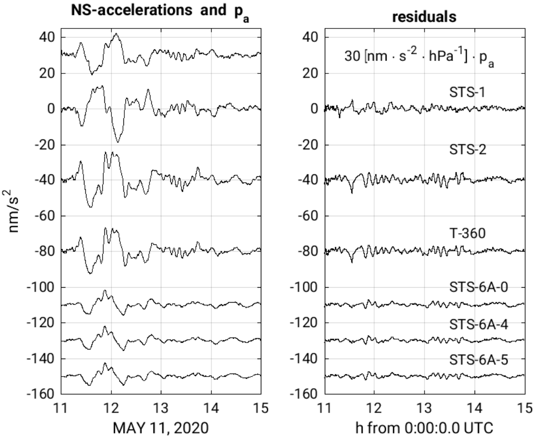

Zürn *et al.* (2021, GJI, vol. 228, 927–943)

Evidence from recorded data

Regression factors

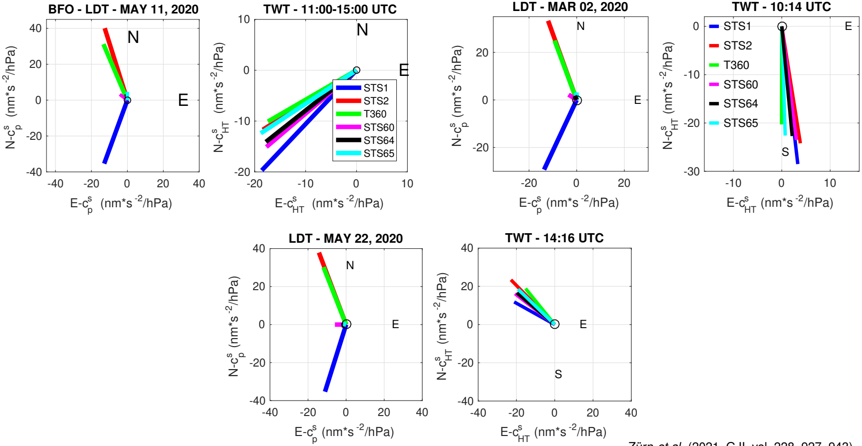

Zürn *et al.* (2021, GJI, vol. 228, 927–943)

Application to Hunga Tonga Lamb- and sound-wave

The Lamb wave signal (1 h – 100 s)

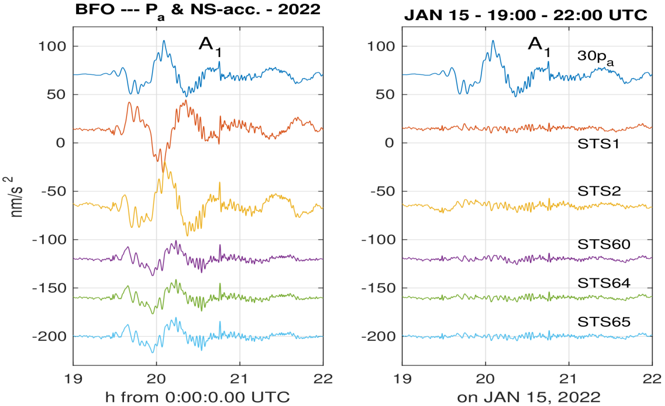

Fig. 10. NS - accelerations vs. barometric pressure. Left panel: same records as in Fig. 4 but for a shorter window with A_1. Right panel: pressure multiplied by 30 c-u and residuals after fitting p_a and HT(p_a) to the accelerograms in the left panel for this window. Broadband sensors are identified in the right panel and in Table 1.

Application to Hunga Tonga Lamb- and sound-wave

The Lamb wave signal (1 h – 100 s)

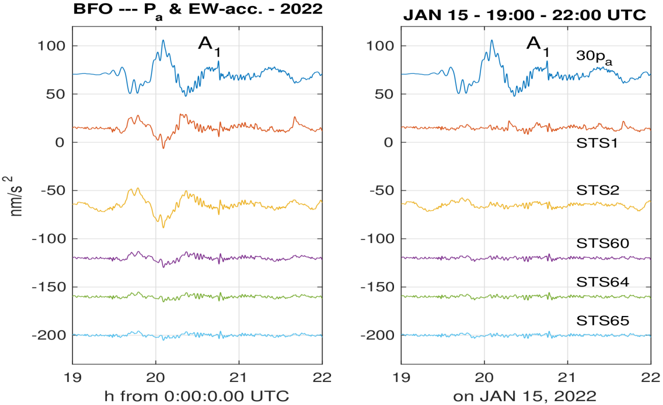

Fig. 11. EW - accelerations vs. barometric pressure. Left panel: same records as in Fig. 5 but for a shorter window with A_1. Right panel: pressure multiplied by 30 c-u and residuals after fitting p_a and $HT(p_a)$ to the accelerograms in the left panel for this window. Broadband sensors are identified in the right panel and in Table 1.

Application to Hunga Tonga Lamb- and sound-wave

Regression coefficients A1 wave

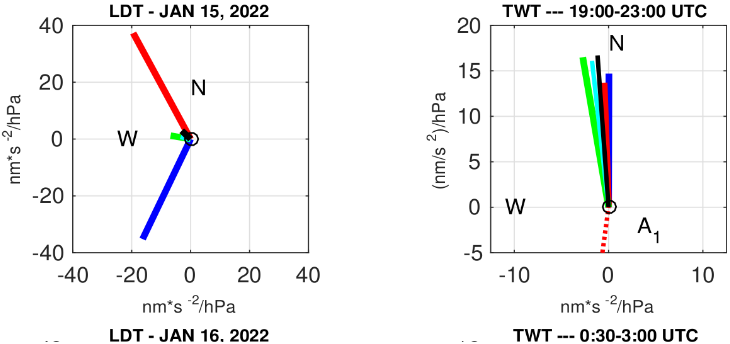

Application to Hunga Tonga Lamb- and sound-wave

Regression coefficients A2 wave

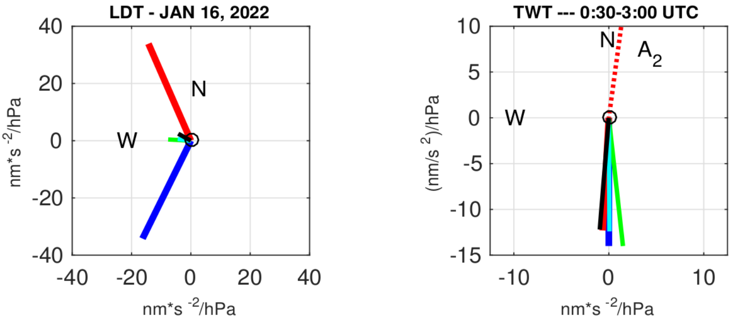

Application to Hunga Tonga Lamb- and sound-wave

The acoustic wave signal (3 mHz – 40 mHz)

Karlsruhe Institute of Technology

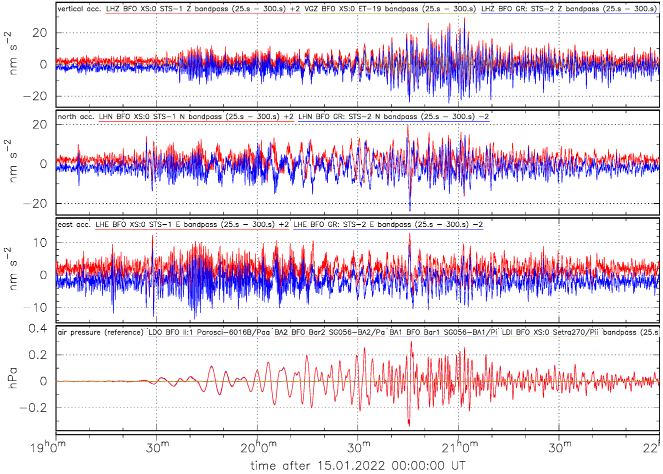

Application to Hunga Tonga Lamb- and sound-wave

The acoustic wave signal (3 mHz – 40 mHz)

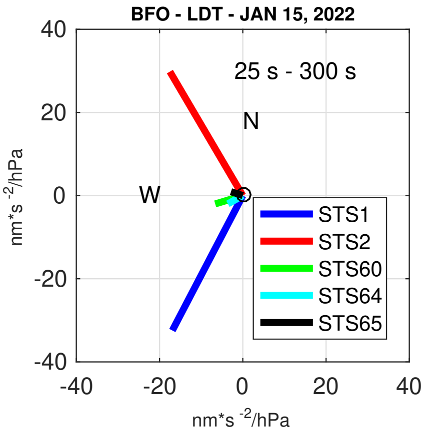

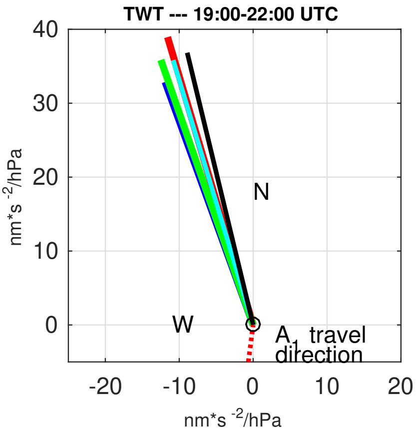

The traveling wave model above 10 mHz

Karlsruhe Institute of Technology

$$\frac{\tilde{a}_h(\omega)}{\tilde{p}(\omega)} = \underbrace{2\pi i \frac{G}{g_0} \frac{1}{1+\frac{\omega c^2}{c_h g_0}}}_{(1)} + \underbrace{i \frac{g_0}{2\mu} \frac{\lambda+2\mu}{\lambda+\mu}}_{(2)} + \underbrace{i \frac{1}{2\mu} \frac{\mu}{\lambda+\mu} \omega c_h}_{(3)}$$

(1): Newtonian attraction (2): tilt-coupled gravity (3): inertial acceleration

- $\tilde{a}_h(\omega)$: Fourier transform of horizontal acceleration
- $\tilde{p}(\omega)$: Fourier transform of air pressure
- G: gravitational constant ($= 6.6743 \times 0^{-11}\,\mathrm{N\,m^2\,kg^{-2}}$)
- g_0: local gravity ($\approx 9.81\,\mathrm{m\,s^{-2}}$)
- c: speed of sound ($\approx 330\,\mathrm{m\,s^{-1}}$)
- λ, μ: Lamé's parameters of homogeneous halfspace
- c_h: horizontal phase velocity ($= \omega/k_h$)

Zürn *et al.* (2007, GJI, vol. 171, 780–796)

The traveling wave model above 10 mHz

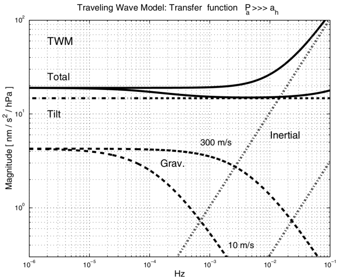

Figure 8. Magnitudes of the transfer-functions between local air pressure and horizontal accelerations for the TWM. Total effect and the three contributions are shown for two values of c_h: 10 and 300 m s^{-1}. $\lambda = \mu = 50$ GPa. The tilt effect is identical for the two cases.

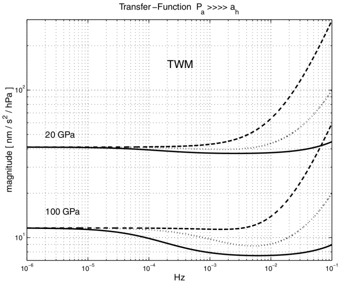

Figure 7. Magnitudes of the transfer-functions between local barometric pressure and horizontal acceleration for the TWM. Solid, dotted, and dashed lines were calculated for $c_\mathrm{h} = 10, 80$ and 330 ms^{-1}, respectively. Two values of $\lambda = \mu$ were used as indicated.

Zürn *et al.* (2007, GJI, vol. 171, 780–796)

Conclusions

Karlsruhe Institute of Technology

- LDT-effect and TWT-effect can be separated in data
- Joint regression with simple models
  provides variance reduction of up to 97 per cent
- Admittance reported by KAGRA is suprisingly large, even if inertial acceleration at frequencies larger than 10 mHz are taken into account
- LDT-type noise can be reduced by method of installation (e. g. posthole)
- With deterministic models local deformation (LDT-type noise) could be identified

Conclusions

Beware of membranes

Karlsruhe Institute of Technology

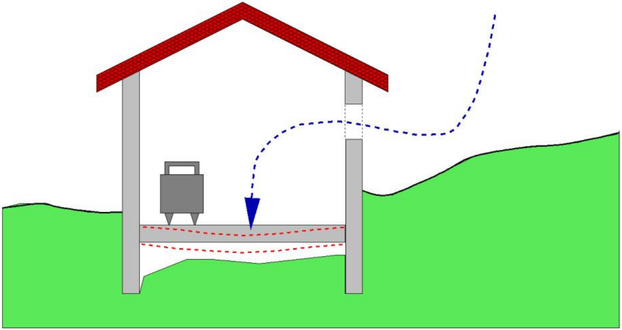

Courtesy of Erhard Wielandt (software-for-seismometry.de)

Thank you for your attention

We are grateful to

- Ruedi Widmer-Schnidrig, Peter Duffner (BFO)
- Adam Ringler, David Kyle Jones, David Wilson (IRIS/USGS, ASL)
- Pete Davis and colleagues (IRIS/IDA)
- Robert Freudenmann (Streckeisen GmbH)
- Sarvesh Upadhyaya (Nanometrics), Steffen Uhlmann (IGM)
- Karl-Heinz Jäckel (GFZ)
- Karin Hafner (IRIS)

References I

Berger, J., P. Davis, and G. Ekström (2004). "Ambient Earth noise: A survey of the Global Seismographic Network". In: *J. Geophys. Res.* 109.B11. online resource, B11307. ISSN: 2156-2202. DOI: 10.1029/2004JB003408.

Gebauer, A., H. Steffen, C. Kroner, and T. Jahr (2010). "Finite element modelling of atmosphere loading effects on strain, tilt and displacement at multi-sensor stations". In: *Geophys. J. Int.* 181.3, pp. 1593–1612. DOI: 10.1111/j.1365-246X.2010.04549.x.

Peterson, J. (1993). *Observations and modelling of background seismic noise*. Open-file report 93-322. online resource. Albuquerque, New Mexico: U.S. Geological Survey. DOI: 10.3133/ofr93322.

References II

Washimi, T., T. Yokozawa, A. Takamori, A. Araya, S. Hoshino, Y. Itoh, Y. Kobayashi, J. Kume, K. Miyo, M. Ohkawa, S. Oshino, T. Tomaru, J. Yokoyama, and H. Yuzurihara (2022). *Response of the underground environment of the KAGRA observatory against the air-pressure disturbance from the Tonga volcano eruption on January 15th, 2022*. DOI: 10.48550/ARXIV.2206.14396.

Zürn, W., J. Exß, S. H., C. Kroner, T. Jahr, and M. Westerhaus (2007). "On reduction of long-period horizontal seismic noise using local barometric pressure". In: *Geophys. J. Int.* 171, pp. 780–796. DOI: 10.1111/j.1365-246X.2007.03553.x.

Zürn, W., T. Forbriger, R. Widmer-Schnidrig, and P. Duffner (2022). "The Hunga Tonga A_1-wave at BFO". In: *Geophys. J. Int.* in preparation.

References III

Zürn, W., T. Forbriger, R. Widmer-Schnidrig, P. Duffner, and A. T. Ringler (2021). "Modelling tilt noise caused by atmospheric processes at long periods for several horizontal seismometers at BFO — a reprise". In: *Geophys. J. Int.* 228.2, pp. 927–943. DOI: `10.1093/gji/ggab336`.

Black Forest Observatory (BFO)

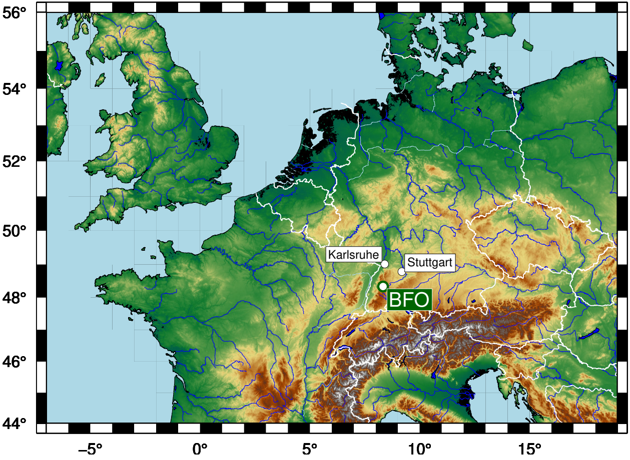

Black Forest Observatory (BFO)

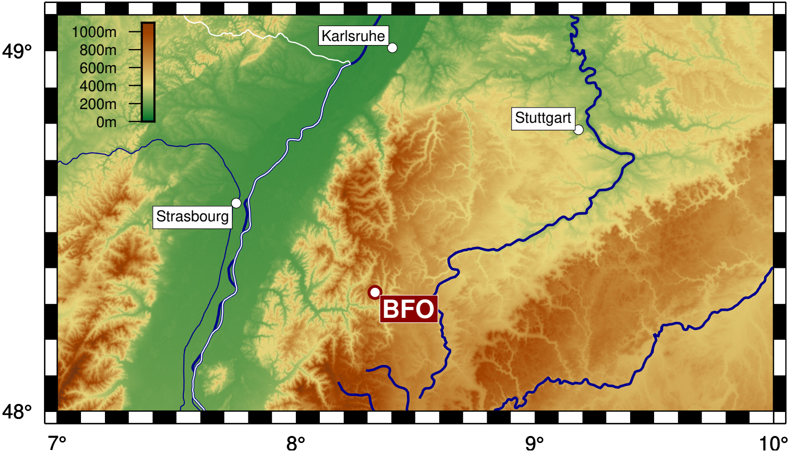

Black Forest Observatory (BFO)

Karlsruhe Institute of Technology

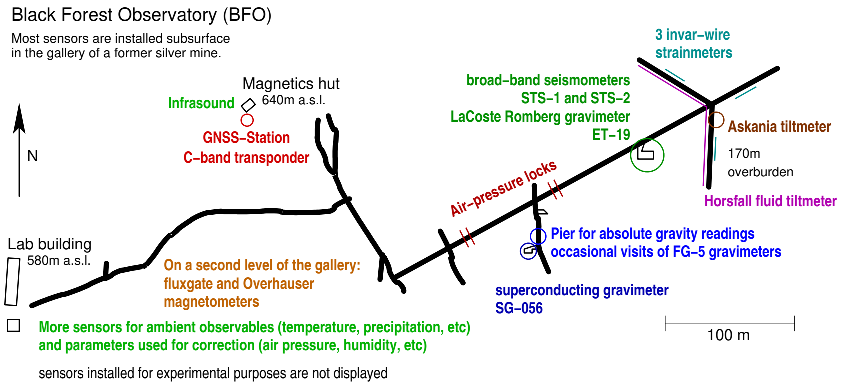

Black Forest Observatory (BFO)

Cross-section of local geology

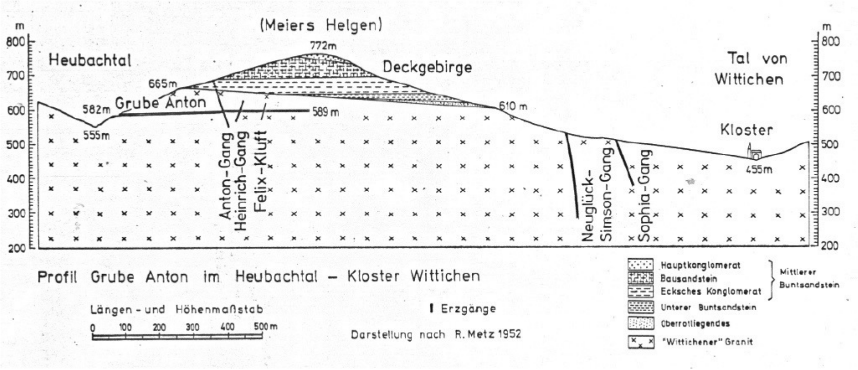

Noise caused by the atmosphere

period band 100 s to 3600 s

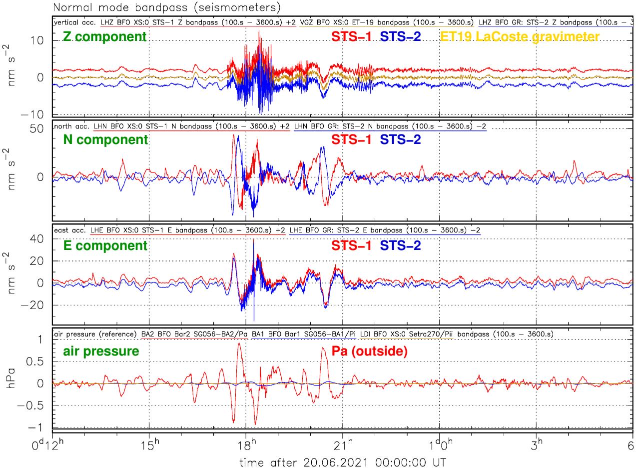

20.06.2021 17:05:51 M6.4 South of Kermadec Islands

Mitigation of atmospheric noise

period band 100 s to 3600 s

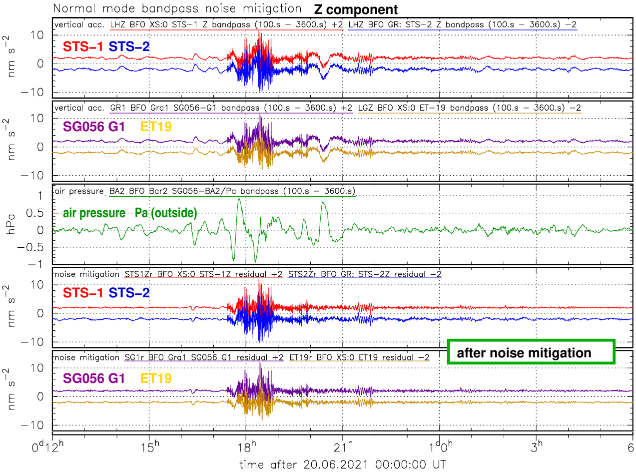

20.06.2021 17:05:51 M6.4 South of Kermadec Islands

Noise caused by the atmosphere

Consistency of polarity

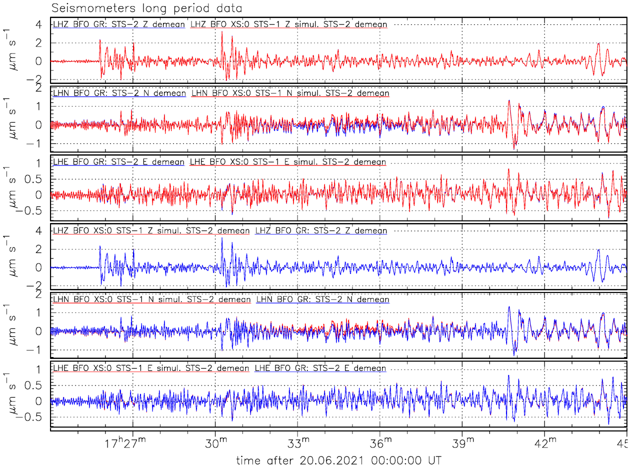

20.06.2021 17:05:51 M6.4 South of Kermadec Islands

Noise caused by the atmosphere

period band 100 s to 3600 s

Karlsruhe Institute of Technology

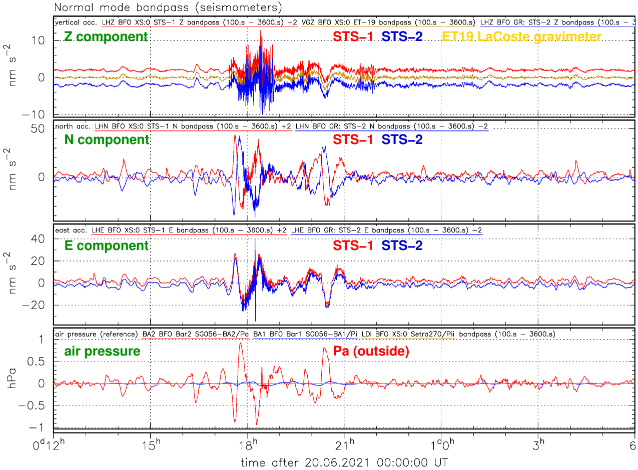

20.06.2021 17:05:51 M6.4 South of Kermadec Islands

Coupling mechanisms
Tilt-coupled gravity

Definition of horizontal component

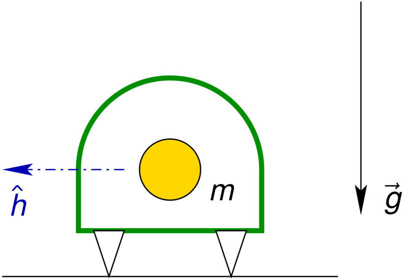

Coupling mechanisms
Tilt-coupled gravity

Response to inertial acceleration

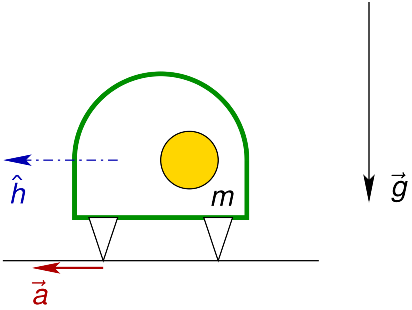

Coupling mechanisms

Tilt-coupled gravity

Response to tilt

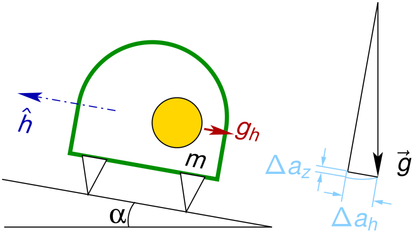

horizontal component

first order effect; $\Delta a_\mathrm{h} \approx |\vec{g}|\,\alpha$

vertical component

second order effect; $\Delta a_z \approx |\vec{g}|\,\alpha^2/2$

$$\alpha \approx 0.000\,000\,001\,\mathrm{rad}$$

$$|\vec{g}| \approx 10\,000\,000\,000\,\mathrm{nm\,s^{-2}}$$

Coupling mechanisms

’Local deformation tilt’ (LDT): cavity deformation

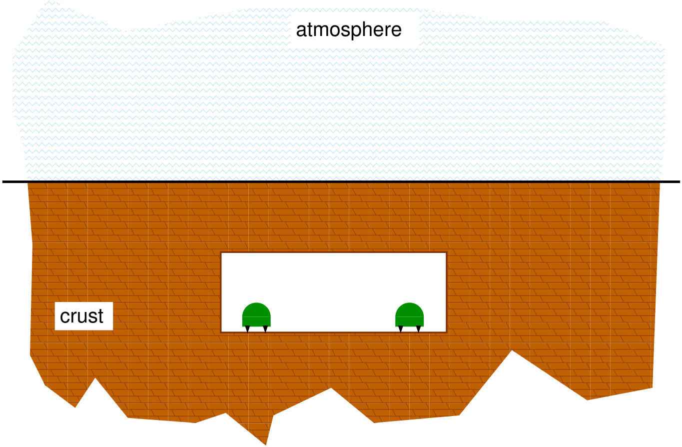

LDT as defined by Zürn *et al.* (2007, GJI, vol. 171, 780–796)

Coupling mechanisms

'Local deformation tilt' (LDT): cavity deformation

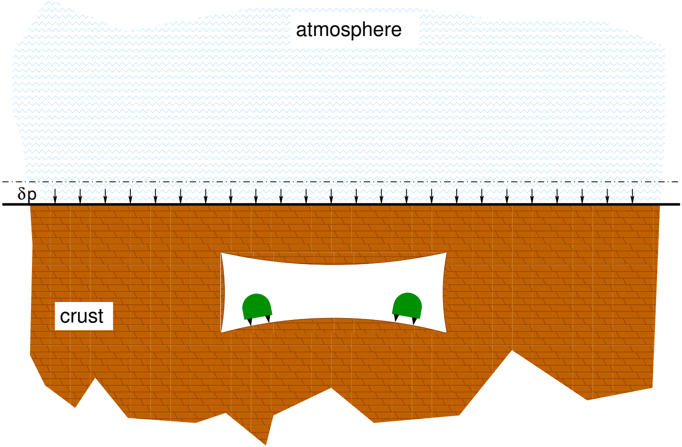

LDT as defined by Zürn *et al.* (2007, GJI, vol. 171, 780–796)

Coupling mechanisms

'Traveling wave tilt' (TWT): horizontal gradient

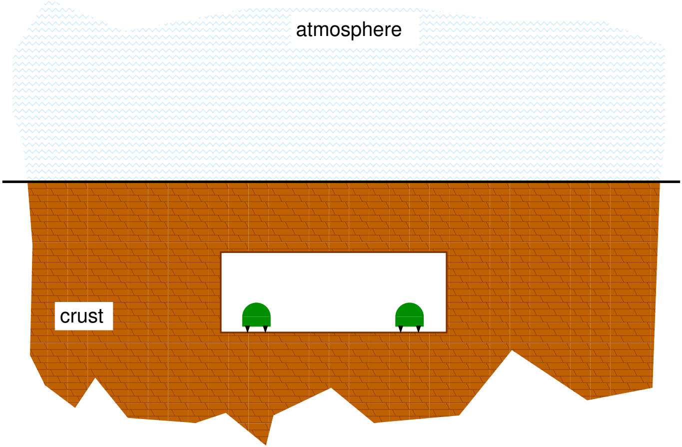

TWT as defined by Zürn *et al.* (2007, GJI, vol. 171, 780–796)

Coupling mechanisms

’Traveling wave tilt’ (TWT): horizontal gradient

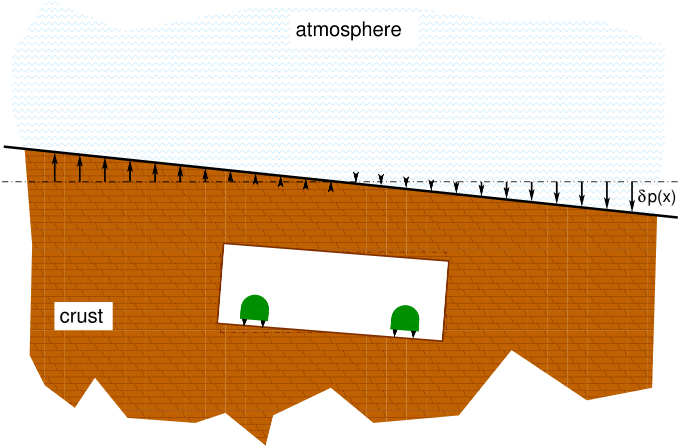

TWT as defined by Zürn *et al.* (2007, GJI, vol. 171, 780–796)

Evidence from recorded data

Instruments selected for this study

Karlsruhe Institute of Technology

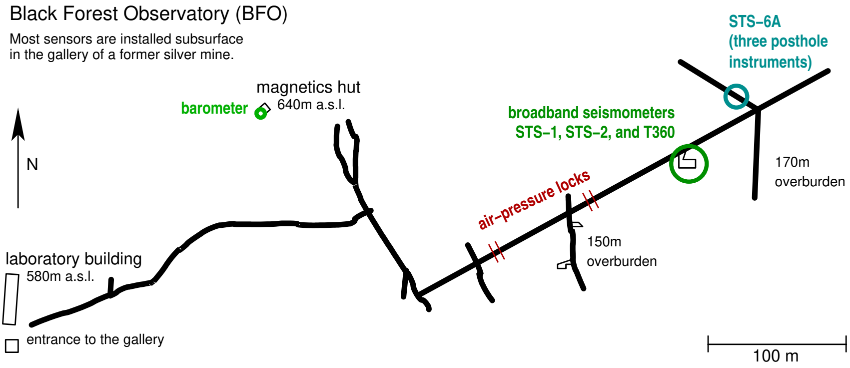

Evidence from recorded data

Instruments selected for this study
Seismometer vault at BFO

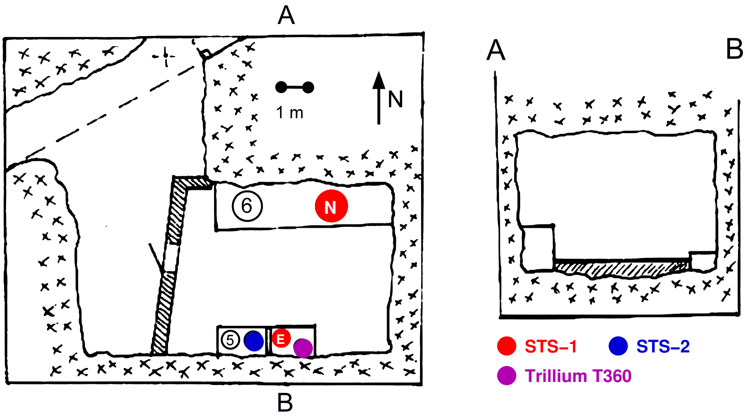

Evidence from recorded data

Instruments selected for this study

Black Forest Observatory (BFO)

Most sensors are installed subsurface
in the gallery of a former silver mine.

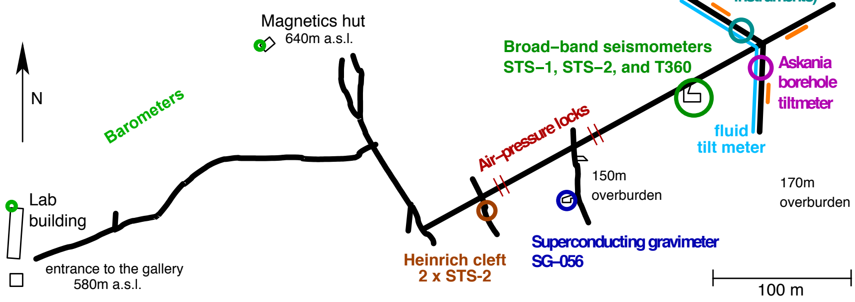

Evidence from recorded data

Joint regression

Karlsruhe Institute of Technology

$$a_h(t) = c_p\, p(t) + c_{\mathrm{HT}}\, \mathrm{HT}\,[p(t)] + r(t)$$

Minimize $r(t)$ in a least squares sense by adjusting c_p and c_{HT}.

$a_h(t)$: horizontal acceleration

$p(t)$: air pressure

c_p: accounts for LDT

$r(t)$: residual

$\mathrm{HT}\,[p(t)]$: Hilbert transform of $p(t)$

c_{HT}: accounts for TWT

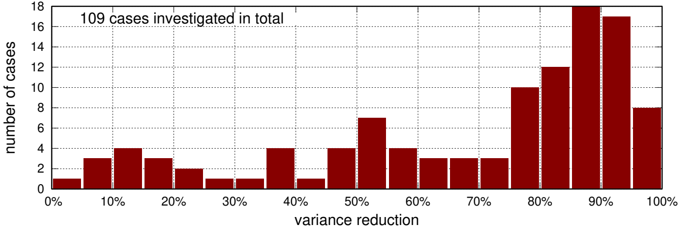

Zürn *et al.* (2021, GJI, vol. 228, 927–943)

Evidence from recorded data

Joint regression

Karlsruhe Institute of Technology

$$a_h(t) = c_p\, p(t) + c_{\mathrm{HT}}\, \mathrm{HT}\left[p(t)\right] + r(t)$$

Minimize $r(t)$ in a least squares sense by adjusting c_p and c_{HT}.

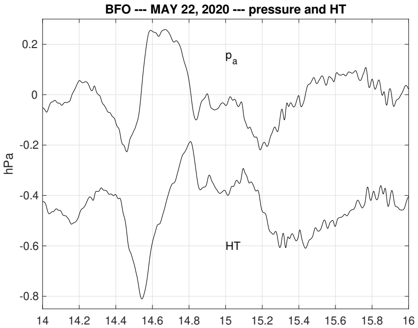

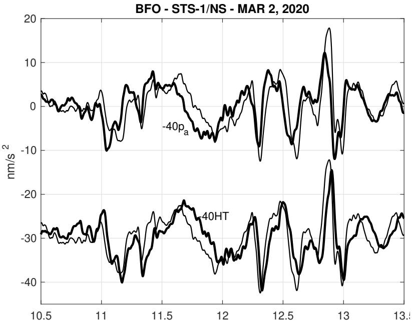

Zürn *et al.* (2021, GJI, vol. 228, 927–943)

Evidence from recorded data

Joint regression

$$a_h(t) = c_p\, p(t) + c_{\mathrm{HT}}\, \mathrm{HT}\,[p(t)] + r(t)$$

Minimize $r(t)$ in a least squares sense by adjusting c_p and c_{HT}.

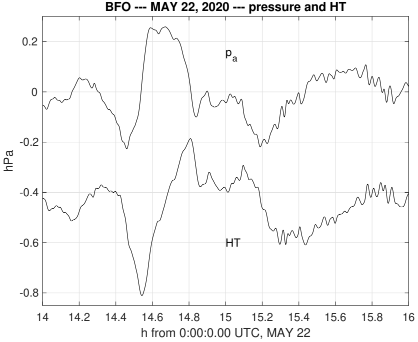

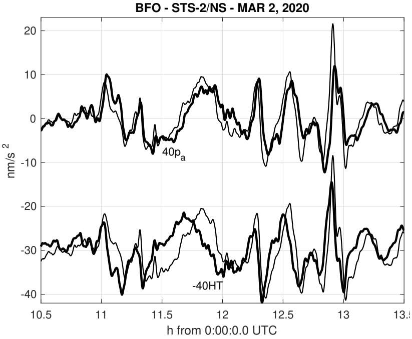

Zürn *et al.* (2021, GJI, vol. 228, 927–943)

Evidence from recorded data

Variance reduction

Date	Windows	Components	STS-1	STS-2	T360	STS-6A-0	STS-6A-4	STS-6A-5	Remarks
04/03/2017	1	N,E	90	94	-	-	-	-	
01/03/2018	3	N	79	77	-	-	-	-	
11/03/2018	4	N	97	97	-	-	-	-	
15/03/2018	2	N	96	93	-	-	-	-	
01/06/2018	1	N,E	84	83	-	-	-	-	ASK 52%
20/10/2019	1	N	88	91	-	-	-	-	
15/11/2019	1	N,E	87	86	84	74	-	-	
16/11/2019	3	N,E	89	89	85	78	-	-	
17/11/2019	1	N,E	89	92	90	78	-	-	STS1/N #2 79%
25/02/2020	3	N	54	74	72	17	19	27	
26/02/2020	1	N	38	47	44	9	10	15	
27/02/2020	1	N	9	22	23	10	10	12	
29/02/2020	2	N,E	57	53	53	63	65	67	
01/03/2020	1	N,E	61	55	52	57	54	49	
02/03/2020	1	N,E	89	88	84	85	85	84	
07/03/2020	1	N	39	55	35	2	31	35	STS1/N #2 9%
11/05/2020	5	N,E	93	95	94	95	95	96	S112 93%, S113 94%
22/05/2020	4	N,E	93	94	95	93	93	93	
23/05/2020	5	N,E	84	87	84	83	83	85	
03/08/2020	1	N,E	93	87	-	86	87	88	
25/09/2020	1	N,E	93	89	-	76	77	77	
05/11/2020	1	N,E	63	66	-	46	50	46	
15/11/2020	1	N,E	78	78	-	83	83	84	

Zürn *et al.* (2021, GJI, vol. 228, 927–943)

Evidence from recorded data

Example of joint regression

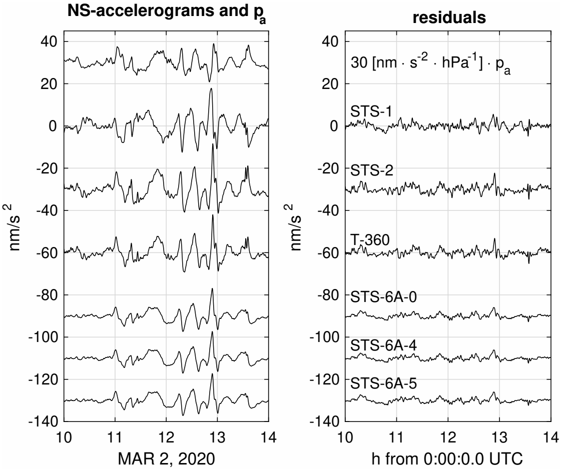

Zürn *et al.* (2021, GJI, vol. 228, 927–943)

Evidence from recorded data

Example of joint regression

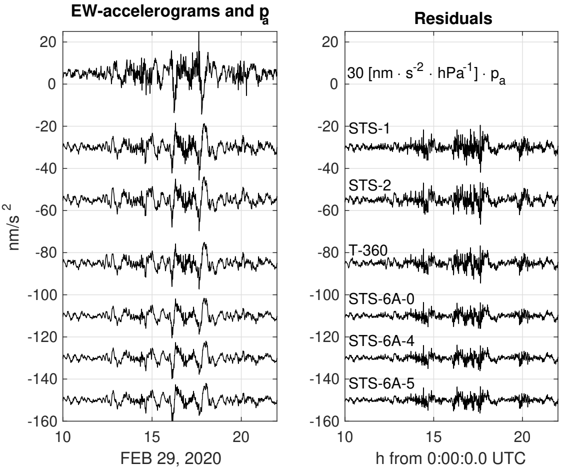

Zürn *et al.* (2021, GJI, vol. 228, 927–943)

Evidence from recorded data

Example of joint regression

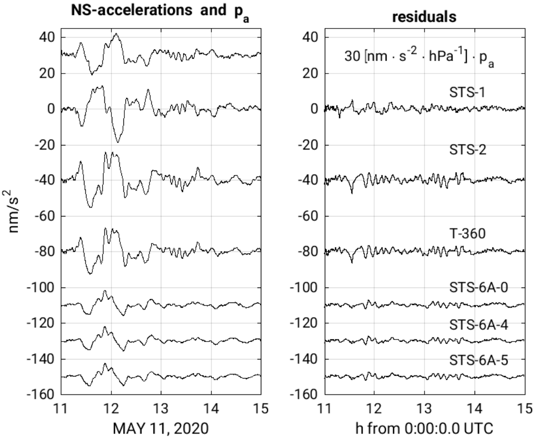

Zürn *et al.* (2021, GJI, vol. 228, 927–943)

Evidence from recorded data
Example of joint regression

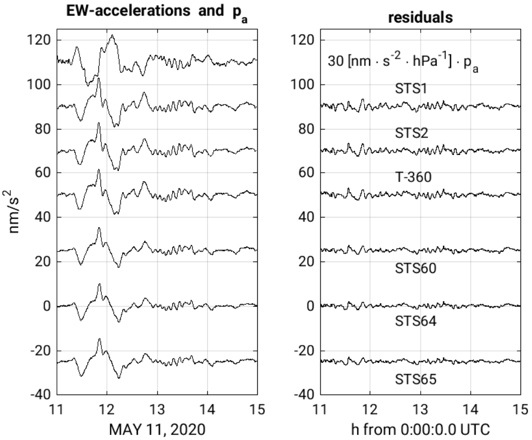

Zürn *et al.* (2021, GJI, vol. 228, 927–943)

Evidence from recorded data

Regression factors

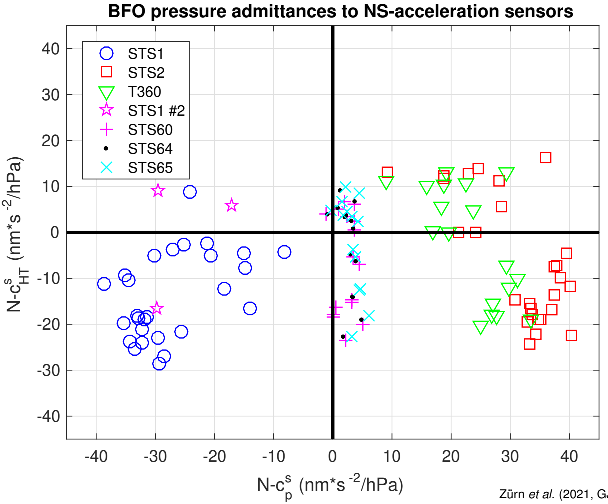

Zürn *et al.* (2021, GJI, vol. 228, 927–943)

Evidence from recorded data

Regression factors

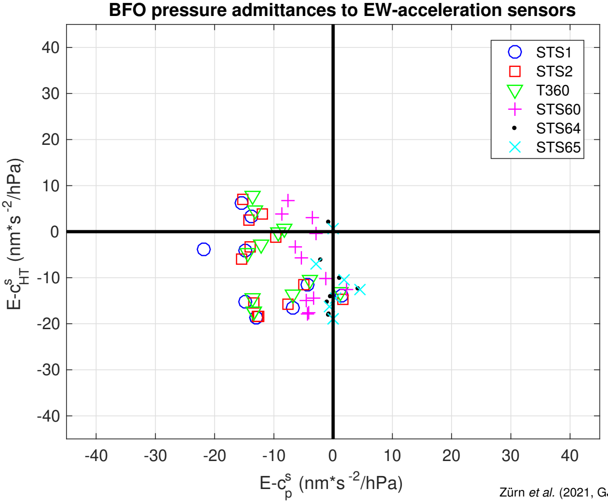

Zürn *et al.* (2021, GJI, vol. 228, 927–943)

Evidence from recorded data
Regression factors

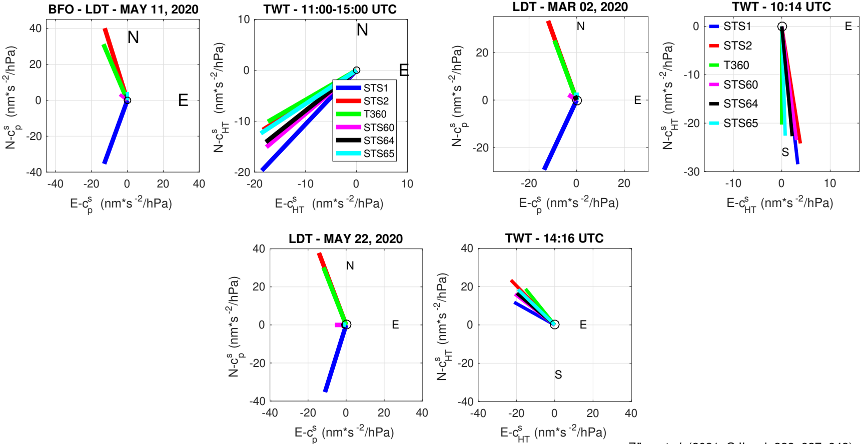

Zürn *et al.* (2021, GJI, vol. 228, 927–943)

Evidence from recorded data
Regression factors

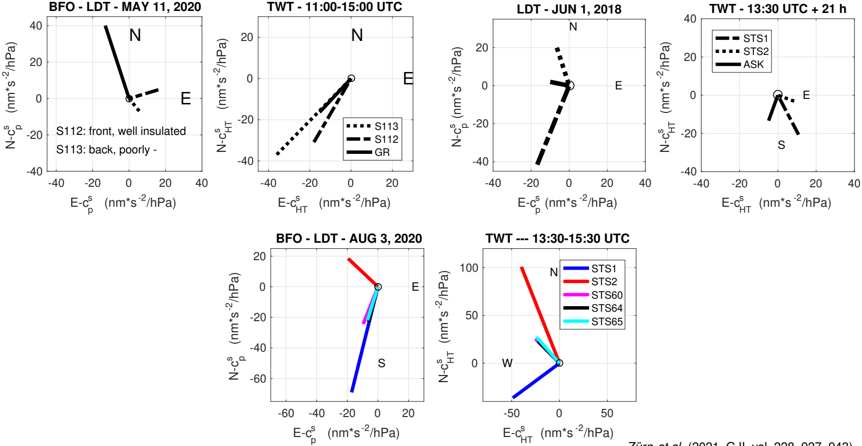

Zürn *et al.* (2021, GJI, vol. 228, 927–943)

Evidence from recorded data

Regression factors compared with FE computation

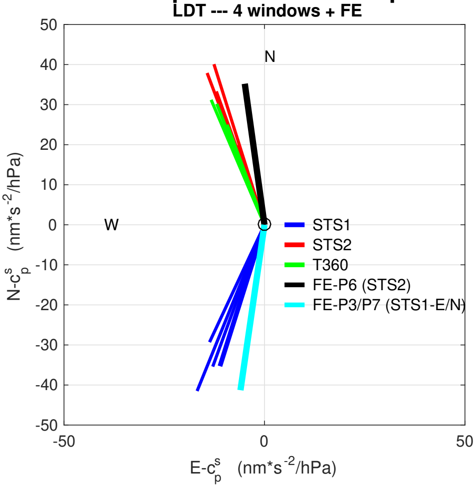

Zürn *et al.* (2021, GJI, vol. 228, 927–943)
Gebauer *et al.* (2010, GJI, vol. 181, 1593–1612)

Hunga Tonga Lamb- and sound-wave

The Lamb wave signal (1 h – 100 s)

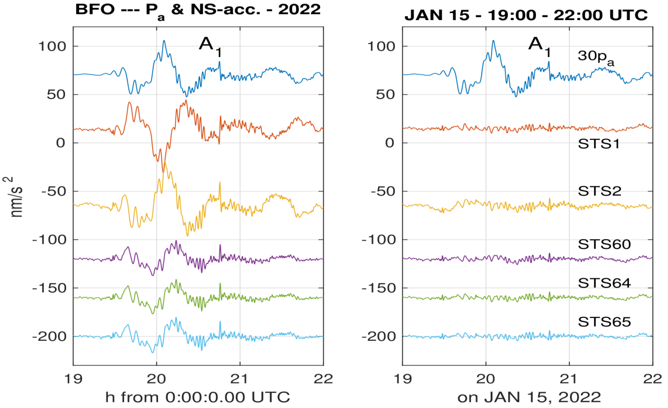

Fig. 10. NS - accelerations vs. barometric pressure. Left panel: same records as in Fig. 4 but for a shorter window with A_1. Right panel: pressure multiplied by 30 c-u and residuals after fitting p_a and $HT(p_a)$ to the accelerograms in the left panel for this window. Broadband sensors are identified in the right panel and in Table 1.

Hunga Tonga Lamb- and sound-wave

The Lamb wave signal (1 h – 100 s)

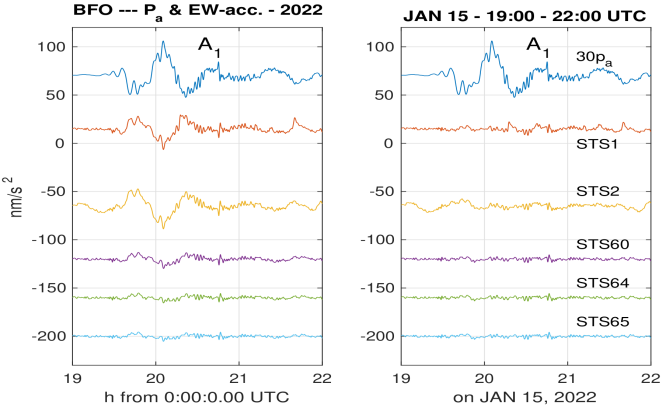

Fig. 11. EW - accelerations vs. barometric pressure. Left panel: same records as in Fig. 5 but for a shorter window with A_1. Right panel: pressure multiplied by 30 c-u and residuals after fitting p_a and $HT(p_a)$ to the accelerograms in the left panel for this window. Broadband sensors are identified in the right panel and in Table 1.

Hunga Tonga Lamb- and sound-wave

The Lamb wave signal (1 h – 100 s)

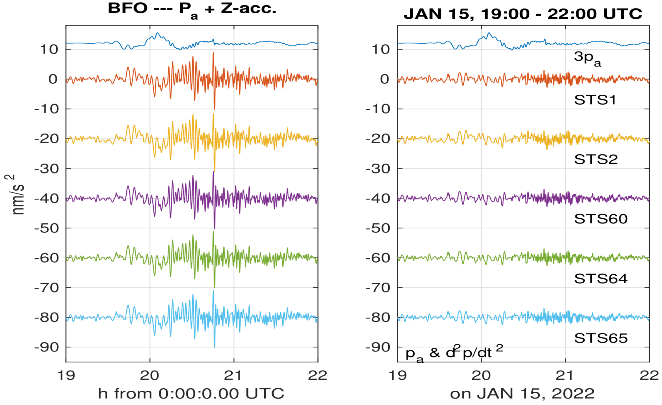

Fig. 13. Vertical accelerations vs. barometric pressure. Left panel: same records as in Fig. 6 but for a shorter window with A_1. Right panel: pressure multiplied by 3.0 c-u and residuals after fitting p_a and $d^2 p_a/dt^2$ to the accelerograms in the left panel for this window. Broadband sensors are identified in the right panel and in Table 1.

Hunga Tonga Lamb- and sound-wave

The Lamb wave signal (1 h – 100 s)

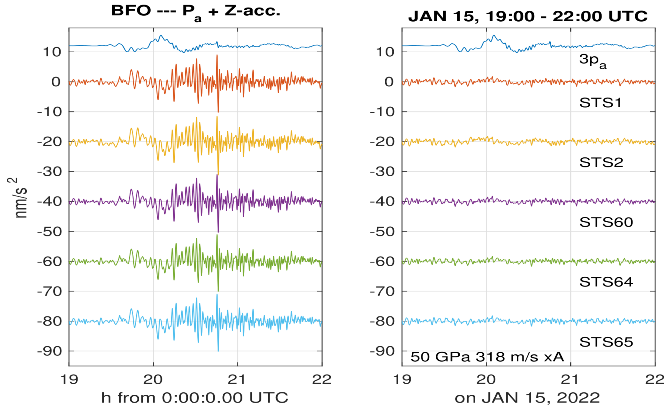

Fig. 15. Same as Fig. 13: Vertical accelerations vs. barometric pressure. However, here the residuals in the right panel were obtained by subtracting a scaled version of the "pressure accelerogram" computed using the TWM with parameters $\mu = 50$ GPa and $c_h = 318$ m/s. The best scale factor in a least squares sense was 1.505. Broadband sensors are identified in the right panel and in Table 1.

Hunga Tonga Lamb- and sound-wave

The Lamb wave signal (1 h – 100 s)

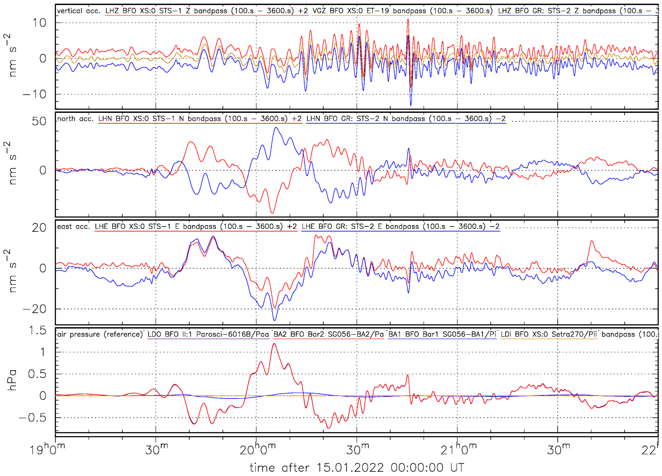

Hunga Tonga Lamb- and sound-wave

Regression coefficients A1 wave

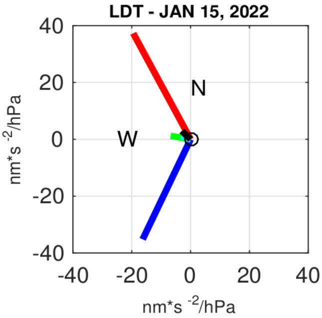

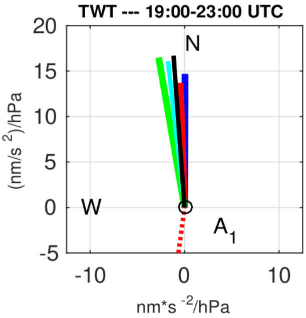

LDT - JAN 16, 2022

TWT --- 0:30-3:00 UTC

Hunga Tonga Lamb- and sound-wave

Regression coefficients A2 wave

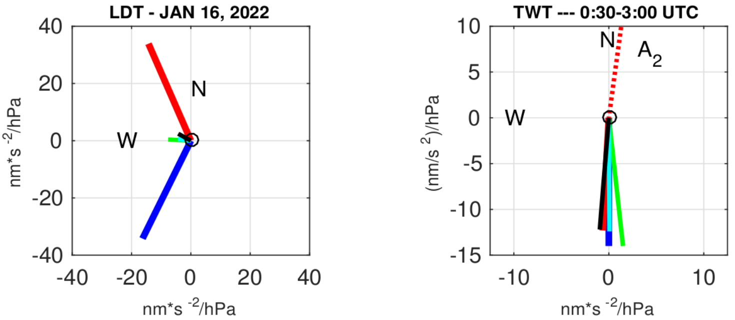

Hunga Tonga Lamb- and sound-wave

The acoustic wave signal (3 mHz – 40 mHz)

Karlsruhe Institute of Technology

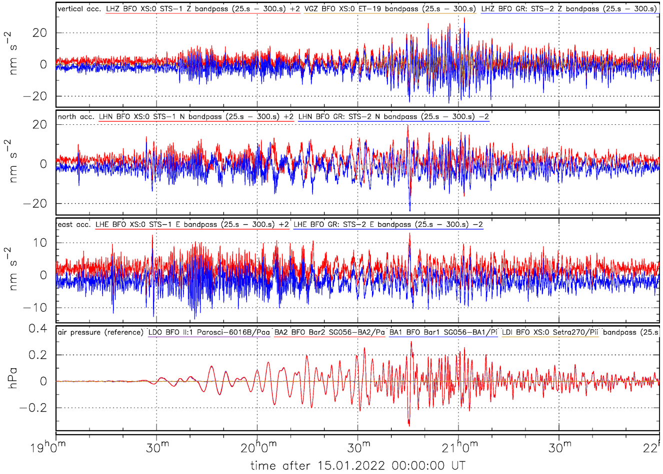

Hunga Tonga Lamb- and sound-wave

The acoustic wave signal (3 mHz – 40 mHz)

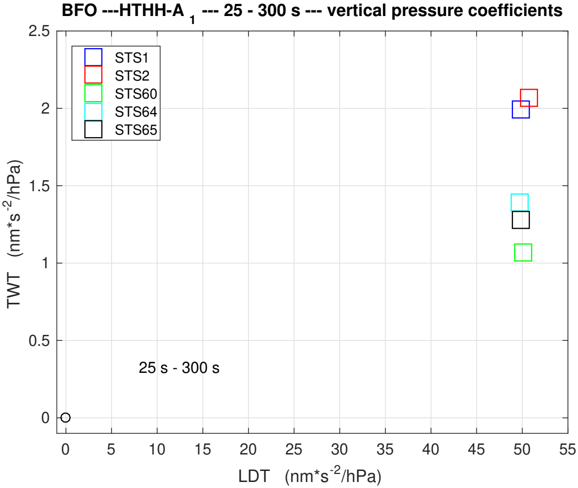

Hunga Tonga Lamb- and sound-wave

The acoustic wave signal (3 mHz – 40 mHz)

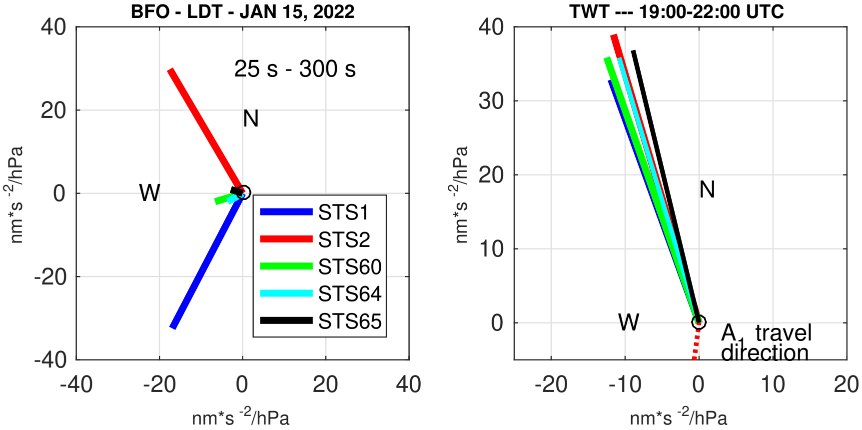

Hunga Tonga Lamb- and sound-wave

3 mHz – 25 mHz

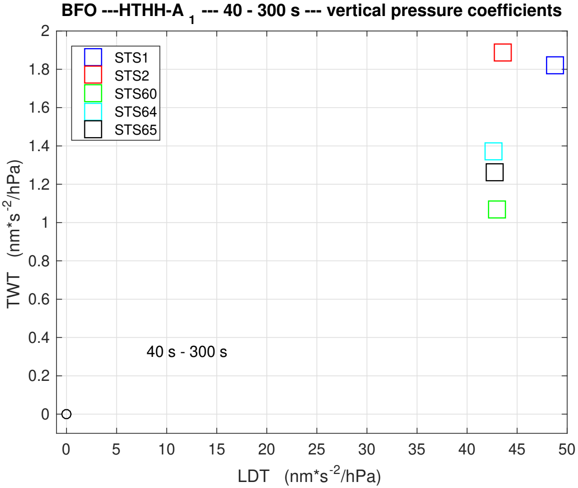

Hunga Tonga Lamb- and sound-wave

3 mHz – 25 mHz

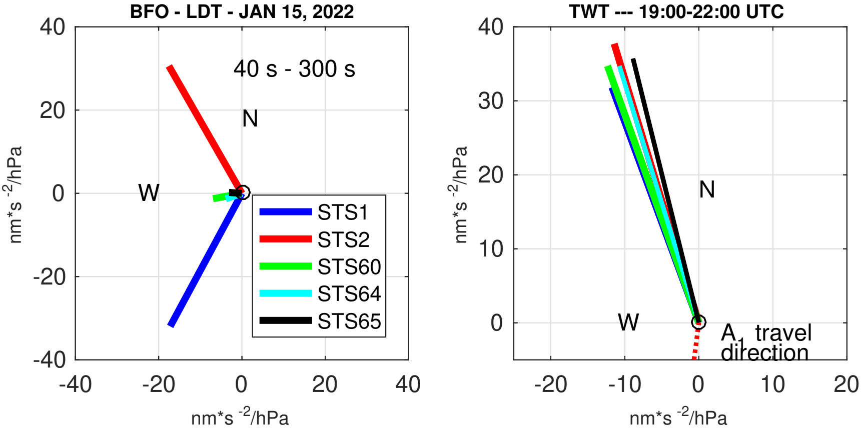

Hunga Tonga Lamb- and sound-wave

3 mHz – 17 mHz

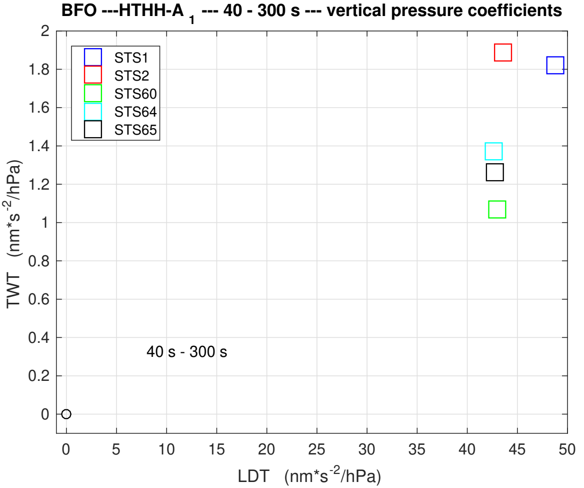

Hunga Tonga Lamb- and sound-wave

3 mHz – 17 mHz

Karlsruhe Institute of Technology

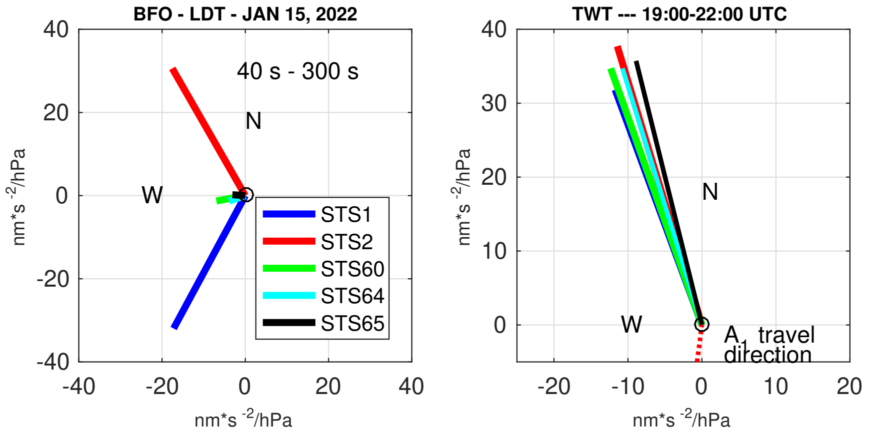

Hunga Tonga Lamb- and sound-wave

3 mHz – 10 mHz

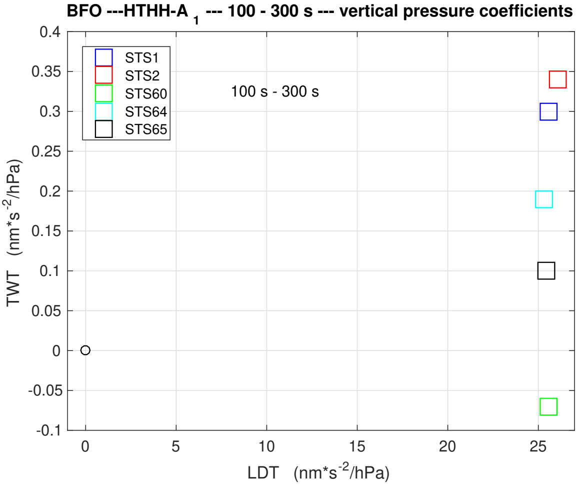

Hunga Tonga Lamb- and sound-wave

3 mHz – 10 mHz

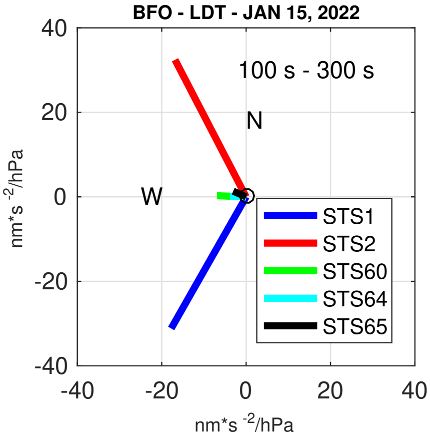

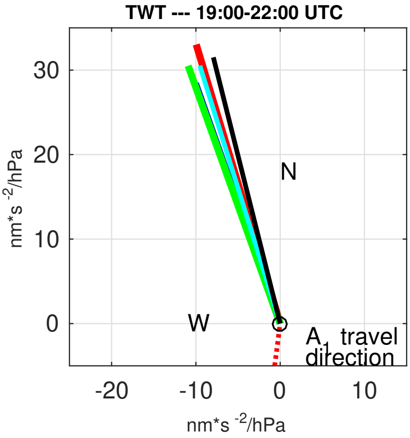

Hunga Tonga Lamb- and sound-wave

Frequency dependence of LDT coeffients

Karlsruhe Institute of Technology

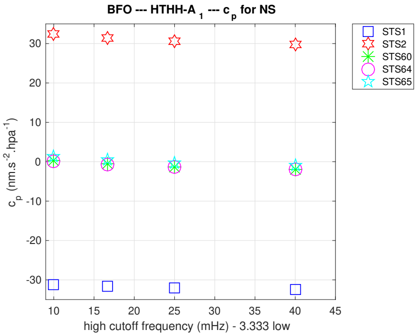

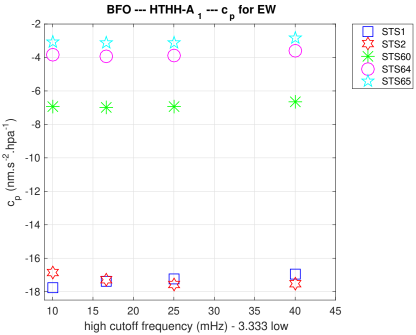

Hunga Tonga Lamb- and sound-wave

Frequency dependence of TWT coeffients

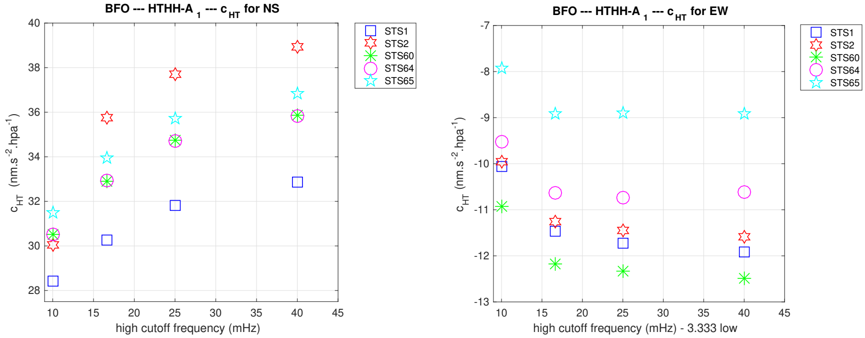

Hunga Tonga Lamb- and sound-wave

Frequency dependence of variance reduction

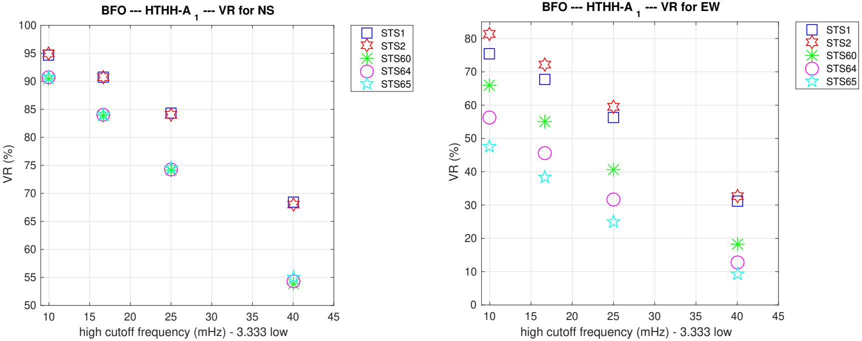

Hunga Tonga Lamb- and sound-wave

Frequency dependence for STS-1

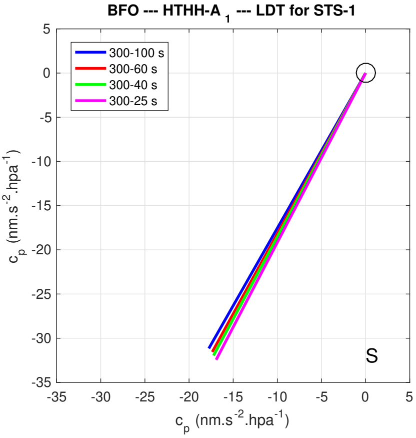

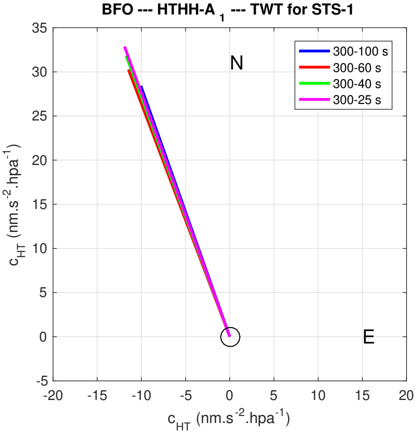

Hunga Tonga Lamb- and sound-wave

Frequency dependence for STS-2

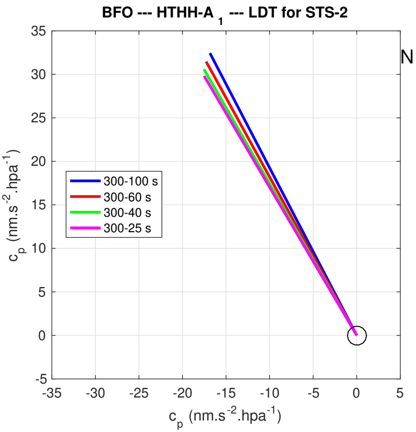

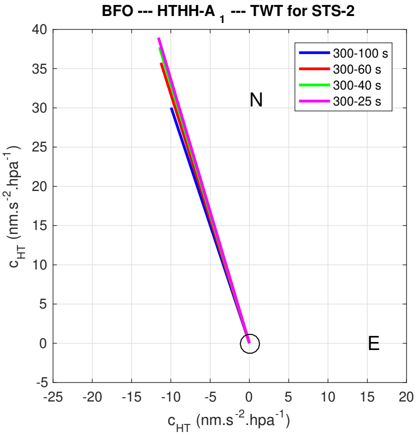

Hunga Tonga Lamb- and sound-wave

Frequency dependence for STS-6A-0 (SN 150804)

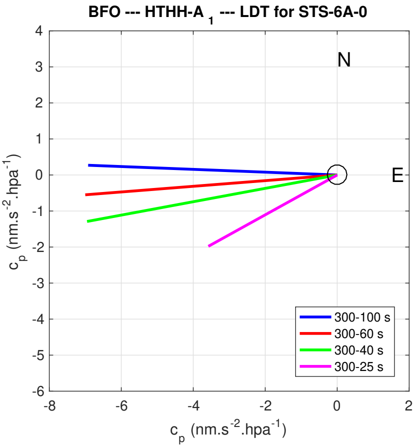

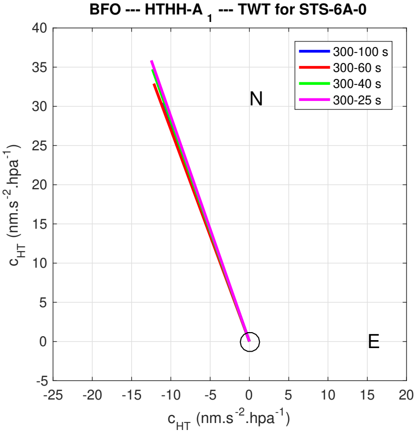

Hunga Tonga Lamb- and sound-wave

Frequency dependence for STS-6A-4 (SN 176241)

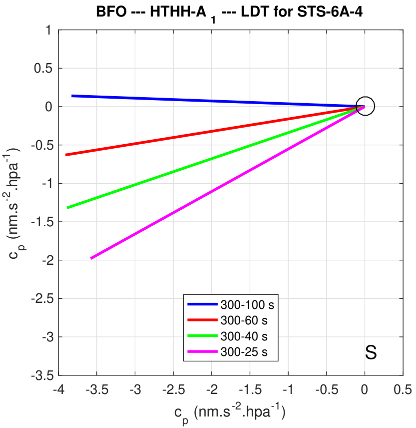

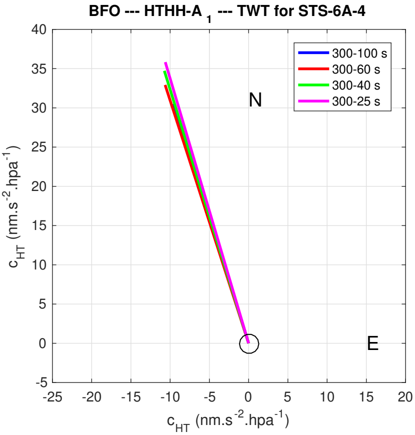

Hunga Tonga Lamb- and sound-wave

Frequency dependence for STS-6A-5 (SN 176254)

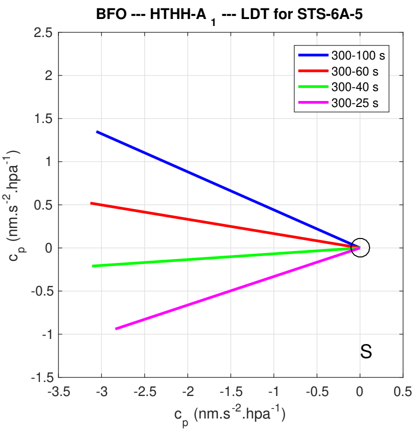

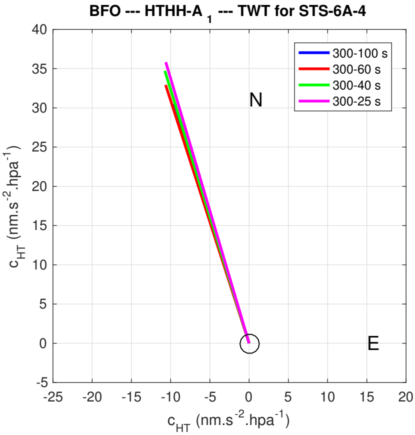

Hunga Tonga Lamb- and sound-wave

Frequency dependence of Z coeffients

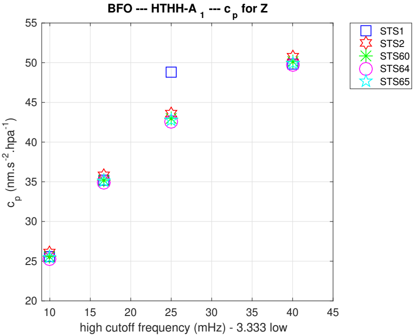

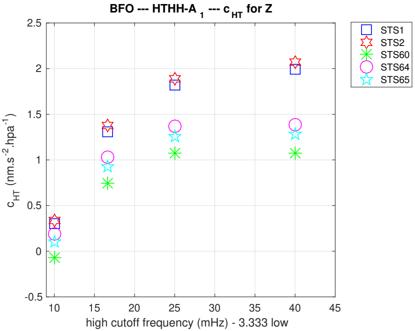

Hunga Tonga Lamb- and sound-wave

Frequency dependence of Z variance reduction